BAMS Article

GeoXO

NOAA's Future Geostationary Satellite System

Daniel T. Lindsey, Andrew K. Heidinger, Pamela C. Sullivan, Joel McCorkel, Timothy J. Schmit, Michelle Tomlinson, Ryan Vandermeulen, Gregory J. Frost, Shobha Kondragunta, and Scott Rudlosky

KEYWORDS:
Atmosphere;
Ocean;
Remote sensing;
Satellite observations

ABSTRACT: Geostationary Extended Observations, or GeoXO, is NOAA's future geostationary satellite constellation, set to launch in the early 2030s and operate into the 2050s. Given changes to the Earth system, improvements in technology, and expanding needs of satellite data users, GeoXO will extend NOAA's current observation suite by adding three new instruments and one new spacecraft. Improved versions of the imager and lightning mapper will again be placed on East and West satellites, where they will monitor severe storms, tropical cyclones, fires, and other hazards. They will be joined by an ocean color instrument designed for detection of harmful algal blooms, phytoplankton, chlorophyll-*a*, and other constituents. The third geostationary spacecraft will be placed in the center of the United States and will carry a hyperspectral infrared sounder, an atmospheric composition instrument, and potentially a partner payload. Radiances from the sounder will be assimilated into numerical weather prediction models to improve forecasts, and sounder-derived retrievals of vertical profiles of temperature and water vapor will allow forecasters to detect and track areas of enhanced instability. Retrievals of pollutants such as nitrogen dioxide and ozone from the new atmospheric composition instrument along with trace gas measurements from the sounder will be used to improve air quality monitoring, forecasts, and warnings in addition to climate monitoring. Once complete, the GeoXO constellation will contribute to an international "geo ring" of satellites that will be used for worldwide weather, oceans, climate, and air quality monitoring. This revolutionary new geostationary satellite constellation will provide critical observations for a changing Earth system.

SIGNIFICANCE STATEMENT: The Geostationary Extended Observations (GeoXO) satellite constellation will provide critical Earth observations for over two decades, feeding numerical models and providing forecasters with the information they need to issue life-saving warnings and forecasts. Extending beyond weather monitoring capabilities, GeoXO will also monitor the oceans and air quality, responding to the needs of a changing climate.

https://doi.org/10.1175/BAMS-D-23-0048.1
Corresponding author: Dan Lindsey, dan.lindsey@noaa.gov
In final form 10 January 2024

AFFILIATIONS: Lindsey—NOAA/NESDIS, Fort Collins, Colorado; **Heidinger and Schmit**—NOAA/NESDIS, Madison, Wisconsin; **Sullivan**—NOAA/NESDIS, Greenbelt, Maryland; **McCorkel**—NASA GSFC, Greenbelt, Maryland; **Tomlinson**—NOAA/NOS, Silver Spring, Maryland; **Vandermeulen**—NOAA/NMFS, Silver Spring, Maryland; **Frost**—NOAA/OAR, Silver Spring, Maryland; **Kondragunta and Rudlosky**—NOAA/NESDIS, College Park, Maryland

The United States began geostationary weather observations in 1966 with the National Aeronautics and Space Administration's (NASA) *Applications Technology Satellite 1* (*ATS-1*), which launched in December of 1966 with the Spin-Scan Cloud Camera that imaged in one visible band (Suomi and Parent 1968). The first Synchronous Meteorological Satellite (SMS) launched in May of 1974 with both visible and infrared imaging capabilities (Goodman et al. 2019, chapter 2). Geostationary observations became operational in 1975 with the launch of the National Oceanic and Atmospheric Administration's (NOAA) *GOES-1*, and since that time there have been 18 satellites in 5 different "generations," with improvements with each generation. The current operational satellite series, GOES-R (Gurka and Dittberner 2001), was launched in 2016 and consists of three on-orbit platforms, GOES-East, GOES-West, and a third spacecraft serving as the on-orbit spare, with a fourth satellite planned for launch in 2024. The GOES-R series will continue to provide NOAA's geostationary observations into the 2030s, and the requirement for an on-orbit spare necessitating a new series of satellites with a first launch in 2032. That is the primary schedule driver for NOAA's future geostationary constellation known as Geostationary Extended Observations (GeoXO).

The NOAA Satellite Observing System Architecture Study (NSOSA; Maier et al. 2021) completed its report in 2018 and evaluated nearly 100 observational architectures, including both low-Earth-orbit (LEO) and geostationary platforms. They also looked at observational alternatives such as leveraging partner data and using commercial data. As part of NSOSA, the NOAA Space Platform Requirements Working Group (SPRWG) published its final report in 2018 (www.nesdis.noaa.gov/sites/default/files/SPRWG_Final_Report_20180325_Posted.pdf; Anthes et al. 2019) in which a set of prioritized observational recommendations were made. Both of these reports were reviewed as a starting point for defining the GeoXO observational requirements.

Early in 2020, a NOAA-wide working group was chartered with a goal of recommending a set of observational requirements for GeoXO. The GeoXO User Requirements Working Group (XORWG) spent most of 2020 on this task, and ultimately delivered its recommendations to NOAA. Given the GeoXO operational timeline, which is expected to extend from the early 2030s to the mid-2050s, it was necessary to evaluate the expected future observational needs given ongoing changes to the Earth, including climate change. A series of themed workshops were held in 2020 to better understand expected future user needs; themes included fires, weather, agriculture and land use, human health, and oceans. Further user input came through surveys, polls, and community meetings. The XORWG also evaluated NOAA line office priorities and gaps in the future observational network. Considerations were given to continuity, risk, technological readiness, spacecraft limitation, partner agency plans, and overall budget constraints. The GOES-R series Earth observations focus mainly on weather applications with its Advanced Baseline Imager (ABI; Schmit et al. 2005, 2018)

and Geostationary Lightning Mapper (GLM; Goodman et al. 2013). For GeoXO, NOAA will continue these observations with some targeted improvements to its imager (GXI) and lightning mapper (LMX), and add support for air quality, oceans, coasts, climate, and enhanced weather prediction capability with three new instruments: a hyperspectral infrared sounder (GXS), an ocean color instrument (OCX), and an atmospheric composition (ACX) instrument. Figure 1a shows the GeoXO constellation. GEO-West and GEO-East spacecraft will continue the long tradition of imager observations at 137° and 75°W. LMX and OCX will join GXI on GEO-West and GEO-East, and a new central spacecraft near 105°W longitude will host GXS and ACX, with space for an additional partner payload. The tentative timeline for launch and operations is shown in Fig. 1b; this is valid as of the writing of this paper, but is subject to change. The Geo-I spacecraft (carrying the imager, lightning mapper, and ocean color instruments) will operate from the GEO-East and -West positions, and the Geo-S spacecraft

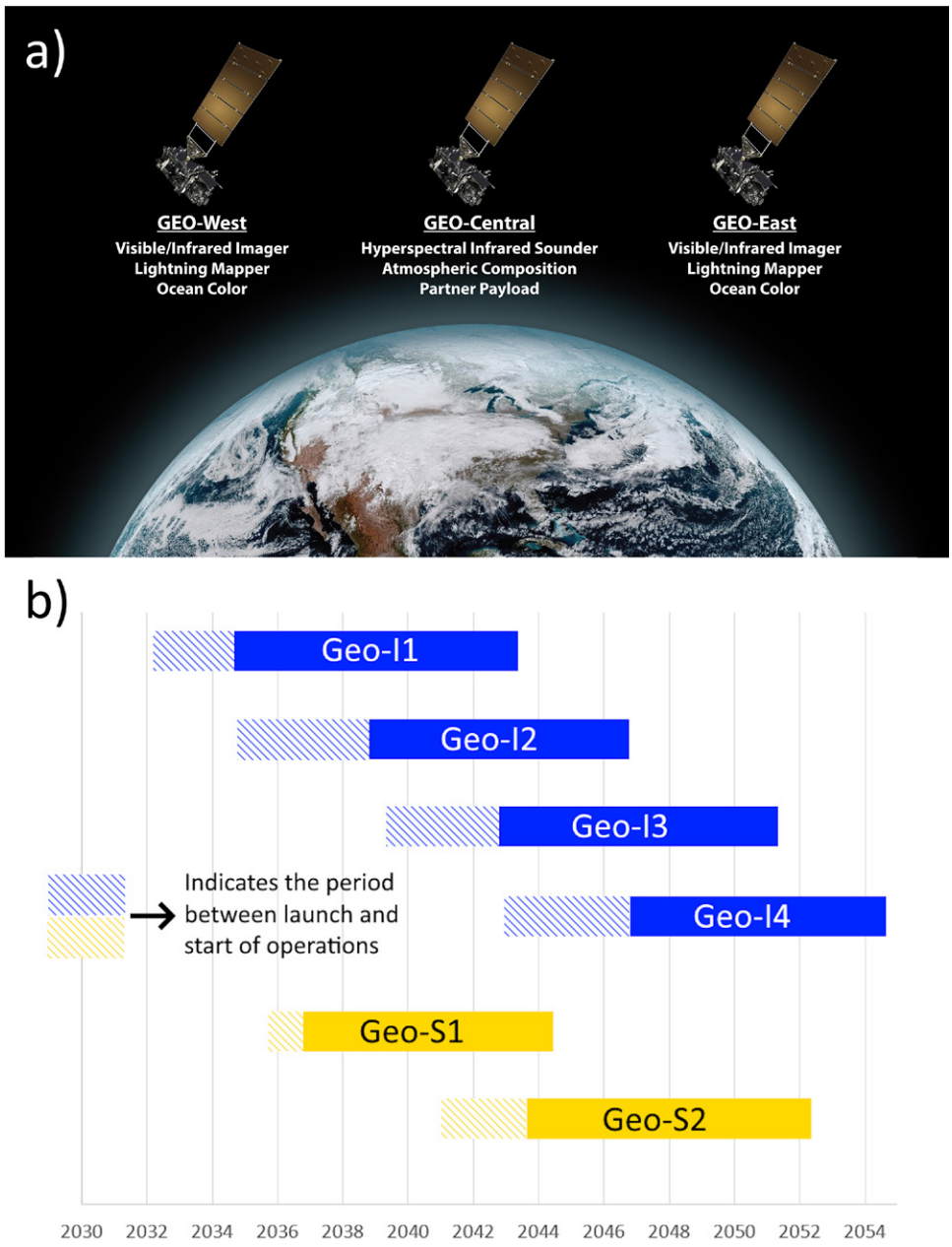

Fig. 1. (a) The GeoXO Constellation indicating which instruments are on which spacecraft. (b) Tentative GeoXO launch and operations timeline, as of the writing of this paper. It is subject to change. The Geo-I spacecraft refers to those that will operate from the GEO-East and GEO-West positions at 75° and 137°W, and the Geo-S spacecraft those that will operate from the GEO-Center position at 105°W.

(carrying the sounder, atmospheric composition, and partner payload instruments) will operate from the GEO-Center position. As shown in Fig. 1b, there will be six total spacecraft, with a maximum of three operating simultaneously, and operations will extend to the mid-2050s. In addition to meeting the needs of NOAA and its users in the United States, GeoXO is consistent with the capabilities outlined by the World Meteorological Organization (WMO) Integrated Global Observing System (WIGOS) 2040 (https://library.wmo.int/idurl/4/66218) and will contribute to the ring of worldwide geostationary meteorological satellites. In this paper we will first provide the details of each of the five GeoXO instruments, then list select applications that the constellation as a whole is expected to provide.

GeoXO instruments

The measurements acquired by GeoXO instruments span wide temporal, spatial, and spectral ranges that were carefully selected to meet mission observational requirements. This section provides a summary of key instrument parameters along with some of the products and applications each instrument will provide.

Imager instrument. NOAA has had continuous coverage from geostationary imagers since *GOES-1* in the mid-1970s to provide real-time observations of severe weather and hazardous environmental conditions. The ABI, currently flying on GOES-East and GOES-West, provides 16 spectral channels with subpoint resolutions ranging from 500 m in the visible to 2 km in the longwave infrared (Schmit et al. 2005). This technology represented a significant upgrade relative to the previous generation of imagers, which had only five channels. When developing requirements for the GeoXO imager (GXI), feedback from the user community indicated that improvements in spatial resolution will provide larger positive observational impact relative to spectral or temporal improvements, but some additional channels were also desired.

Table 1 shows the 18 channels that GXI will have on the right side, along with the 16 channels from ABI on the left, with central wavelength, bandwidth, and subpoint pixel size comparisons. Green shaded boxes indicate additions or improvements relative to ABI. Seven channels will have improved resolution by approximately a factor of 4 (2 times in each pixel direction), including a 250 m visible channel, which is aimed at better resolving small-scale clouds such as cumulus along boundaries and will assist a forecaster in pinpointing the time and location of convective initiation. The pixel dimensions listed in Table 1 are equivalent to the sampling distance, i.e., resolution, of the data. GXI will also have 1 km pixels in the window IR 10.35 μm channel and the 6.95 μm water vapor channel. It is worth noting that the modulation transfer function (MTF) requirements are equivalent to 1.5 km pixels for these two channels due to expected difficulties in achieving actual 1 km resolution. Despite this, these advancements are expected to allow for better depictions of storm-top features, improved fog detection at night, and better detection of atmospheric gravity waves that may cause aircraft turbulence.

Fire detection has become an increasingly important application given increased wildfire activity (Westerling 2016). To help address early detection, the resolution of the 3.9 μm channel will be improved from a 2 km pixel to a 1 km pixel, resulting in pixels that are a factor-of-4 finer relative to ABI. Also, considering that sub-pixel-sized fires can be detected with 3.9 μm imaging (Weaver et al. 2004), the improved spatial resolution of GXI will enable smaller fires to be seen, allowing earlier detection and subsequent alerts.

The two new channels that GXI will offer relative to ABI are designed for improved detection of low-level water vapor: 0.91 and 5.15 μm. The 0.91 μm channel follows the lead of EUMETSAT's new Flexible Combined Imager (FCI; Holmlund et al. 2021), which was launched aboard the Meteosat Third Generation (MTG) *Imager-1* (*MTG-I1*) spacecraft in December 2022.

Table 1. GeoXO Imager (GXI) channel specifications (right) compared to the GOES-R Advanced Baseline Imager (ABI) channels (left), taken from Schmit et al. (2017). Green shading represents additions or improvements relative to the ABI. NIR stands for near infrared.

	GOES-R Advanced Baseline Imager			GeoXO GXI		
Channel range	Central wavelength (μm)	50% bandwidth (μm)	Pixel dimensions at nadir (km)	Central wavelength (μm)	50% bandwidth (μm)	Pixel dimensions at nadir (km)
VIS	0.47	0.040	1.0	0.47	0.040	0.5
VIS	0.64	0.086	0.5	0.64	0.10	0.25[a]
NIR	0.86	0.035	1.0	0.86	0.039	0.5
NIR				0.91	0.020	1.0
NIR	1.37	0.014	2.0	1.38	0.015	2.0
NIR	1.6	0.045	1.0	1.61	0.060	1.0
NIR	2.2	0.046	2.0	2.25	0.050	1.0
IR	3.9	0.19	2.0	3.90	0.20	1.0
IR				5.15	0.20	1.0
IR	6.2	0.80	2.0	6.19	0.83	2.0
IR	6.95	0.42	2.0	6.95	0.40	1.0[b]
IR	7.33	0.19	2.0	7.34	0.20	2.0
IR	8.4	0.44	2.0	8.50	0.40	2.0
IR	9.6	0.38	2.0	9.61	0.38	2.0
IR	10.3	0.30	2.0	10.35	0.50	1.0[b]
IR	11.2	0.79	2.0	11.20	0.80	2.0
IR	12.3	0.92	2.0	12.30	1.00	2.0
IR	13.3	0.57	2.0	13.30	0.60	2.0

[a] Modulation Transfer Function (MTF) equivalent to 0.3 km pixel size.
[b] MTF equivalent to 1.5 km pixel size.

Located in the near-IR (NIR) spectrum with no emitted component from the Earth, and within a water vapor absorption line, this channel is sensitive only to water vapor and surface albedo (and not temperature), which simplifies its interpretation. The 5.15 μm channel lies on the spectrally cleaner shortwave side of the water vapor absorption region that extends from roughly 5–8 μm, and has a vertical weighting function that peaks lower in the atmosphere relative to the ABI legacy 6.2, 6.95, and 7.3 μm channels (Miller et al. 2022; Weisz and Menzel 2022). Combined, these two new channels will improve forecaster's ability to detect and track low-level water vapor, a critical ingredient for severe storms.

The GXI is capable of scanning the Full Disk at least every 10 min, the contiguous United States every 5 min and smaller regions every 30 s or 1 min.

Lightning mapper instrument. Geostationary lightning sensors have optimal spatial and temporal coverage for monitoring thunderstorms, providing data where other sources are more limited, especially over oceans and in mountainous areas. GOES-R's Geostationary Lightning Mapper (GLM) was the first such near-infrared optical sensor in geostationary orbit, and is currently used to detect, locate, and measure the intensity, duration, and extent of lightning flashes. Rapidly updating lightning data can allow forecasters to visualize the intensification of thunderstorms early in their development, often at a faster cadence than radar volume scan updates. Using GLM data alongside radar has increased forecast confidence for warnings, and the improved warnings help reduce casualties (Rudlosky et al. 2020). Space-based lightning imagers are able to depict the initiation and full propagation of lightning flashes (sometimes over tens to hundreds of kilometers; Montanyà et al. 2022) across the

Table 2. Potential LMX improvements relative to GLM, baseline GLM values, and justification for their consideration.

Attribute	GOES-R Geostationary Lightning Mapper	GeoXO Lightning Mapper[a]	Justification
Coverage	East–West GLM full disk (~54°N/S)	East–West GLM full disk extended north	Provide coverage for both CONUS and OCONUS applications
Spatial resolution	~8 km (at the satellite subpoint)	~4 km (at the satellite subpoint)	More precisely locate and portray lightning activity
Temporal resolution	2 ms (500 Hz) frame time	1–2 ms (500–1,000 Hz) frame time	Observe more lightning and better distinguish false events
Signal to noise ratio	~4	>4	Improve instrument performance (both detection efficiency and false alarm rate)
Latency	<20 s	<20 s	Optimally convey rapidly updating lightning information

[a] The GeoXO LMX remains in the initial design phase and specifics on the coverage, spatial resolution, temporal resolution, and signal-to-noise ratio remain to be determined.

hemisphere, augmenting ground-based lightning detection systems whose detection efficiencies are typically much lower over the open ocean, for example. Additional applications are listed in the "Applications" section and more comprehensively in Rudlosky et al. (2020).

The GeoXO Lightning Mapper (LMX) will continue critical observations provided by the GOES-R Series Geostationary Lightning Mapper (GLM) with several potential improvements (Table 2). Primary improvements include finer spatial and temporal resolution, increased signal to noise ratio, and an expanded field of view to include Alaska. Finer resolution and improved signal to noise will allow the LMX to observe smaller and dimmer optical signals than the GLM, which will improve the detection efficiency. Depending on the specific design of the selected instrument, additional improvements could be realized through technological advancements. One key difference would be the use of more modern CMOS (Complementary Metal-Oxide Semiconductor) imaging sensors which will eliminate several CCD (Charge Coupled Device) related artifacts present in the GLM data. The Lightning Imager (LI; Holmlund et al. 2021) on board the MTG-I satellites includes several potential LMX improvements, including CMOS sensors and a spatial resolution of 4.5 km at satellite subpoint.

Ocean color instrument. Rounding out the instruments on the GEO-West and GEO-East satellites, an ocean color instrument in geostationary orbit will provide powerful capability to monitor dynamic oceanographic features in valuable coastal and lake ecosystems. The current capacity for ocean monitoring from satellites provides infrequent coverage: while LEO satellites repeat their ground track once per day, in practice, the effects of cloud cover and sun glint can limit useful observations to once per week in many areas. The GeoXO ocean color instrument (OCX) will greatly improve this observational cadence, providing information with a 2–3 h repeat over the U.S. Exclusive Economic Zone (Fig. 2), consistent with the time scales of many coastal and oceanic processes. Furthermore, the OCX will improve spectral and spatial coverage compared to today's operational LEO sensors: OCX will have hyperspectral resolution, with 10–20 nm band spacing, and ~400 m spatial resolution (Table 3).

The combined capabilities of the OCX instrument represent a logical and significant progression in the technological capabilities utilized for ocean color remote sensing. Current ocean color observations in coastal regions are largely inadequate for many water clarity/quality applications, as input to ecosystem and fishery production models, or for monitoring and forecasting contaminants or harmful algal blooms (HABs) and other pathogens. User requirements and scientific literature consistently point toward the need for higher spatial (Aurin et al. 2013), spectral (Dierssen et al. 2021; Vandermeulen et al. 2017), temporal (IOCCG 2012;

Ruddick et al. 2014; Jolliff et al. 2019), and operational (Groom et al. 2019) observations to adequately understand the mechanisms underlying ecosystem response to change. Technologically, a persistent challenge is that the ocean is a dark target relative to land or clouds, as it only accounts for ~3%–8% of the top-of-atmosphere signal. Thus, the ability to dwell from a geostationary orbit is the only feasible way we can optimize all of these resolutions simultaneously to meet the needs of ocean applications.

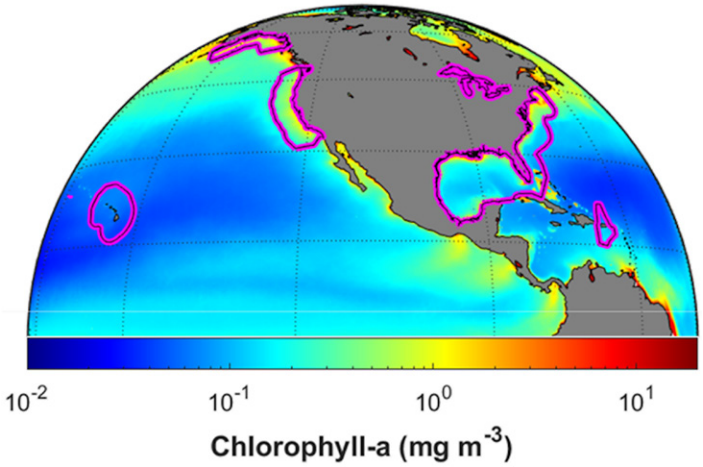

Fig. 2. The proposed sampling plan for OCX (outlined in pink) covers the U.S. Economic Exclusive Zone, to be revisited with a 2–3 h cadence daily. U.S. East Coast–Great Lakes targets will be covered by GeoXO East, and the West Coast–Hawaii targets will be covered by GeoXO West.

Hyperspectral infrared sounder instrument. *GOES-8* through *GOES-15*, operating from the mid-1990s into the late 2010s, included an infrared sounder (Schmit et al. 2002), but it provided low-spectral-resolution observations, which limited its vertical resolutions and consequently usefulness (Schmit et al. 2009). NOAA will improve this situation with the introduction of a hyperspectral Sounder on GeoXO. NOAA and partner organizations have used hyperspectral infrared data since the Atmospheric Infrared Sounder (AIRS; Aumann and Pagano 1994) launched on the low-Earth-orbit *Aqua* satellite in 2002. Several iterations of LEO hyperspectral infrared instruments have launched since then, including the Cross-track Infrared Sounder (CrIS; Glumb and Predina 2002) on the Joint Polar Satellite System (JPSS) series, measuring hundreds to thousands of narrow spectral samples of radiance emitted from the Earth in spectral regions that are sensitive to variations in atmospheric temperature, humidity, and other atmospheric constituents. The atmospheric information unique to sufficiently narrow samples provided by these hyperspectral infrared instruments are used in retrieval algorithms and numerical weather prediction (NWP) models to substantially benefit numerous applications that depend on knowledge of the state of the atmosphere and weather prediction (Menzel et al. 2018). While LEO hyperspectral information provides benefit to global NWP, some limitations prevent it from being as useful for regional NWP and nowcasting. With only a few polar passes per day,

Table 3. Key baseline performance metrics of OCX.

Measurement parameters	GeoXO OCX Performance
Spatial resolution	~400 m (at nadir)
Coverage area	Exclusive Economic Zone (EEZ) East (coast out to EEZ around CONUS plus near CONUS regions of Caribbean, including Puerto Rico, Gulf of Mexico, and the Great Lakes)
	EEZ West (coast out to EEZ around CONUS West Coast plus EEZ Hawaii plus portion of southern Alaska)
Revisit time	3 h during daylight (2 h for EEZ East plus 1 h for Great Lakes)
Spectral band	Hyperspectral (~20 nm resolution and ~10 nm resolution at 680 nm; with at least two spectral samples per resolution element)
	0.350–0.890 μm
SNR	≥600:1 between 0.350 and 0.890 μm, with achievable SNR reported up 1.02 μm

Table 4. GeoXO Infrared Sounder (GXS) primary measurement parameters.

Measurement parameter	GXS performance	Rationale
Coverage	At least 62° local zenith angle	Uncertainties increase substantially at increasing slant angles
Spatial resolution	4 km at the satellite subpoint	Increased cloud-free field-of-view samples at higher resolution
Temporal update	At least 60 min "sounding disk"	Rapid refresh for weather model initial conditions; also commandable for custom timelines and spatial coverage
Longwave IR spectral range	680–1,095 cm^{-1}; 9.13–14.7 μm	Vertical temperature, LWIR window, ozone, NH_3, isoprene, HNO_3, low-level moisture
Short-to-midwave IR spectral range	1,689–2,250 cm^{-1}; 4.44–5.92 μm	Vertical moisture, window and temperature, N_2O, CO
Spectral resolution	Equivalent of 0.625 cm^{-1}	Critical to attain the required vertical resolution for moisture and temperature, etc.

significant temporal gaps exist during which changes can and do occur in preconvective environments. Additionally, data latency is generally at least 1 h with LEO data, too long to be of great value to forecasters who are monitoring quickly changing environments. Therefore, observations with low latency and with temporal refresh of at least hourly are needed to maximize the observational benefit of hyperspectral infrared information; both of these are provided by such an instrument in geostationary orbit.

Building on the value realized from LEO-based infrared measurements, the GeoXO infrared sounder, GXS, will be NOAA's first geostationary-based hyperspectral infrared instrument and will be placed on the GEO-Center satellite (Fig. 1a). The geostationary vantage point allows dramatically improved temporal refresh and spatial resolution performance relative to contemporary LEO-based hyperspectral instrument as shown in Table 4 (from 14 km with CrIS to 4 km at nadir from GXS), and the spectral coverage of GXS along with GXI is shown in Fig. 3. The benefits and performance expectations of the future GXS were studied and guided by the XORWG and thoroughly documented in Adkins et al. (2021). Special Observation System Simulation Experiments (OSSEs) designed to assess the impact of adding a GXS-like instrument

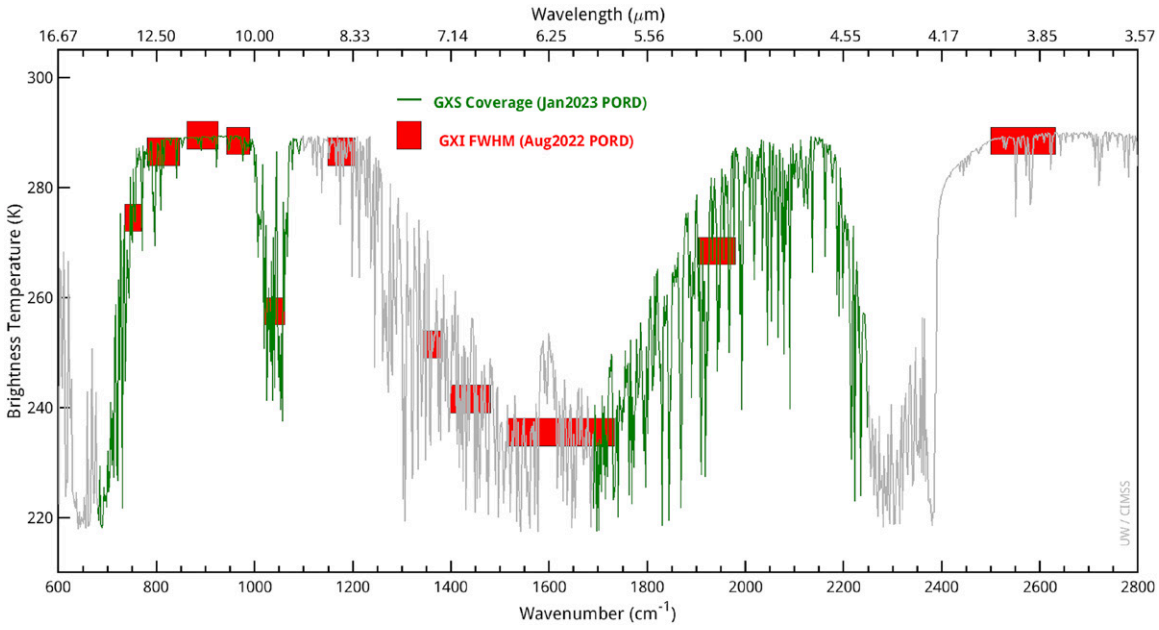

Fig. 3. Spectral coverages in the infrared region of both the GXS (green) and GXI (red bars) as listed in their Performance and Operational Requirements Document (PORD). Courtesy of M. Gunshor, UW/CIMSS.

to the global observing system showed statistically significant (90% level) forecast error reduction past 3 days for temperature and 4 days for moisture (McGrath-Spangler et al. 2022). In fact, when just considering the CONUS domain, the GXS was shown to have the most impact of any satellite sensor for total wet energy regarding the 24-h Forecast Sensitivity Observation Impact (E. McGrath-Spangler et al. 2024). Figure 4 illustrates the approximate spatial coverage of the GXS Sounding Disk (inner oval) relative to two GXIs. There are other (not shown) possible GXS scan patterns, for example, possibly the scanning a truncated Northern Hemisphere, but twice as often providing more information on atmospheric motions over the contiguous United States. Despite the field of view of GXS being limited to a portion of the western hemisphere, the GeoXO GXS will be part of the planned "geo ring" of hyperspectral infrared sounders circling the Earth in geostationary orbit with other sounders provided by China, Europe, Japan, and possibly others.

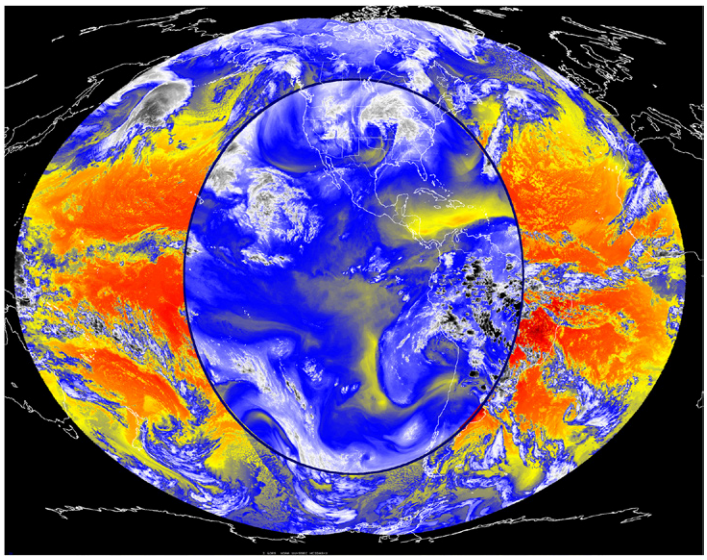

Fig. 4. One scan scenario (center oval) for the GXS each hour, compared to the spatial coverage of the two GXIs. To generate this image, *GOES-17* ABI was used to represent the GXS coverage (to 62 local zenith angles) and *GOES-18* and *-16* ABIs were used to represent GXI (to 85 local zenith angles). The data were mapped into a Mollweide projection.

Atmospheric composition instrument. There is a long history of trace gas and aerosol observational capabilities from ultraviolet–visible hyperspectral instruments in low-Earth orbit for air quality, atmospheric chemistry, and climate applications (Streets et al. 2013; Tong et al. 2015; Duncan et al. 2010; Zhu et al. 2016; Ziemke et al. 2019; Silvern et al. 2019; Jin et al. 2020; Quesada-Ruiz et al. 2020; Kondragunta et al. 2021, 2023). More recently, path-breaking satellite sensors such as the Geostationary Environment Monitoring Spectrometer (GEMS) and the Tropospheric Emissions: Monitoring of Pollution (TEMPO) instruments were launched into geostationary orbit by the Korean Aerospace Research Institute and U.S. National Aeronautics and Space Agency (NASA) in 2020 and 2023, respectively. GEMS and TEMPO extend the trace gas and aerosol measurement capabilities regionally from daily to hourly time scales (Kim et al. 2020; Zoogman et al. 2017). Additionally, the Sentinal-4 UV-VIS-NIR (UVN) spectrometer will fly aboard the second MTG satellite, providing trace gas measurements over Europe in geostationary orbit (Courrèges-Lacoste et al. 2017). The GeoXO ACX instrument, whose specifications are highlighted in Table 5, will be an operational follow-on to TEMPO whose observations will allow NOAA to meet various Congressional, executive, and diplomatic mandates (Frost et al. 2020).

ACX will be a hyperspectral instrument with 0.6 nm spectral resolution, allowing for the retrieval of fine absorption features exhibited by various trace gases between 300 and 500 nm with the first ACX detector in the ultraviolet (see Table 5; Kim et al. 2020; Zoogman et al. 2017). The second ACX detector in the visible has spectral coverage between 540 and 740 nm and covers the oxygen B-band absorption region, which allows for aerosol layer height retrievals (Nanda et al. 2020; Chen et al. 2021). ACX will provide enhanced air quality information compared to the current NOAA geostationary satellite Advanced Baseline Imager (ABI).

Table 5. GeoXO ACX attributes with justifications for why these attributes were selected.

Measurement parameter	GeoXO ACX performance	Rationale
Coverage	CONUS, southern Canada, northern Mexico, Caribbean	Hourly inputs to national air quality, hazard, and fire forecasting capabilities and warnings
Spatial resolution	8 × 3 km^2 at nadir	Resolve sources, including cities, highway corridors, airports, oil/gas fields, large point sources like fires and power plants
Temporal resolution	60 min	Capture diurnal variations in pollution emissions, photochemistry, and exposure; detect episodic events like wildfires and volcanoes
		Select for cloud-free conditions
		Increase geographic coverage compared with LEO or surface observations
Spectral coverage/ resolution	UV: 300–500 nm	Ozone, nitrogen dioxide, formaldehyde, sulfur dioxide, absorption aerosol optical depth
	Vis: 540–740 nm	Cloud/aerosol layer height, PBL ozone, vegetation.
	Both at 0.6 nm	

In general, instruments such as ABI, whose primary purpose is to observe weather can also help with the detection of hazards and tracking hazards such as wildfire smoke, and chemical explosions. The ACX instrument will detect various trace gases including ozone in the stratosphere which protects living organisms from harmful UV radiation and ozone near the surface that is harmful to human health. Other trace gases that will be measured by ACX, such as nitrogen dioxide, are either pollutants themselves or lead to ozone and particle formation. In addition to trace gases, the ACX instrument will also measure aerosol optical depth and aerosol composition, which are good proxies for fine particulate pollution. Additional information from the ACX instrument will include the vertical structure of fine particulate pollution, which can show that pollution is either near the ground, where it directly impacts humans, or higher in the atmosphere where it affects weather and climate.

Applications

Hurricane and severe storm monitoring. Geostationary satellite information is particularly important for storm system monitoring over the open ocean due to the lack of ground-based radar data there. Operational forecasters rely heavily on imagery to detect tropical cyclones (TC) undergoing genesis, estimate TC intensity, assign TC center location and motion, and assess environmental information such as dry air and vertical wind shear. GXI's very-high-resolution visible channel (Table 1) will provide better definition of low-level clouds, and the new 0.91 and 5.15 μm channels will provide more information about layer water vapor in the areas around the storm. Additionally, data from GXS will be assimilated into both regional and global NWP models, leading to improved TC track and intensity forecasts. Lightning observations have been shown to improve TC forecasts for rapid intensification (Stevenson et al. 2018), and rapid intensification forecasting models will leverage total lightning (i.e., intracloud and cloud-to-ground) observations from LMX over the tropical Atlantic and Pacific Oceans where other lightning observations are limited.

Low-level water vapor is a key ingredient for severe storms, and GXS and GXI will both offer significant improvements in the characterization of the prestorm water vapor profile. Spatially sparse radiosonde launches occur regularly only at 1200 and 0000 UTC, and over the United States storms typically form between 1800 and 0000 UTC during this observational gap. Geostationary observations at low latency are ideal for filling in these gaps so that near-storm-environment convective fields such as convective available potential energy (CAPE) and convective inhibition (CIN) can be calculated and tracked with time in order to

assess the potential for convective initiation and subsequent storm severity. GXS data assimilation is also expected to improve NWP wind field forecasts (Eyre et al. 2022), which can have important implications for assessing environments favorable for supercell and tornado formation. Computer simulations have shown that over the CONUS region, the GXS will be the most influential observation system. Lightning observations from LMX will be used by operational forecasters to assist with severe storm warnings, and for advising outdoor event evacuations.

Fires and smoke. With wildfires becoming larger and more frequent in recent years (e.g., Williams et al. 2019), early detection of fires is increasingly important. GXI will provide improved resolution of its primary fire detection channel, 3.9 μm, from 2 to 1 km at nadir (Table 1) relative to ABI. This is a factor-of-4 improvement in pixel size, meaning a smaller fire or a fire with a lower temperature relative to the background can be detected earlier with the better resolution instrument. With GXI data latency expected to be on the order of a few minutes, earlier detection of newly started fires may in some cases allow first responders sufficient time to smother the fire before it grows too large to control.

In addition to the fires themselves, the smoke aerosols produced by fires can be hazardous. Air quality forecast models require accurate information about fire location and intensity, making accurate real-time fire detection even more important. Minimizing the prediction of false alerts and maximizing the prediction of exceedances ($PM_{2.5} > 35\ \mu g\ m^{-3}$) is critical to the forecast models to enable local governments to provide accurate forecasts and take appropriate actions to protect public health. Fires also notoriously have a significant diurnal variation associated with meteorology (Li et al. 2022). Prototype online Community Multiscale Air Quality (CMAQ) model simulations carried out using hourly fire emissions for August 2019 over CONUS showed that surface $PM_{2.5}$ values predicted were accurate with a very small mean bias ($0.169\ \mu g\ m^{-3}$) and root-mean-square error ($3.485\ \mu g\ m^{-3}$), including an accurate prediction of the number of exceedances. In addition to the air quality forecast models, visible channels on GXI will be used to detect and track wildfire smoke in real time, allowing for accurate and timely air quality warnings to be issued to the public.

Air quality. In the GeoXO era, a multi-instrument strategy involving ACX, GXI, and GXS will be employed to use observations relevant to air quality monitoring and forecasting. Table 6 highlights specific application areas and the corresponding observables from GeoXO instruments that will support them. Individual observables are given different typefaces to indicate which instrument will provide this information. Air quality kills tens of thousands of people each year in the United States at an estimated cost of $500 billion to $1,300 billion (GBD 2019 Risk Factors Collaborators 2020). Air quality forecasters who provide alerts rely on near-real-time satellite imagery, ground observations, and National Weather Service (NWS) numerical forecast guidance for ozone and $PM_{2.5}$. (https://airquality.weather.gov/).

Emissions data are key inputs to the NWS air quality forecast models. Considerable uncertainty remains in both model inputs, such as emissions inventories and model processes, limiting these models' capability to accurately forecast air quality. To accurately model emissions with high spatiotemporal variability, there is a need for more advanced, process-based emissions models that can be combined with near-real-time (NRT) satellite data. GeoXO's ACX, GXI, and GXS will provide hourly data on air pollutants, including nitrogen dioxide, ozone, formaldehyde, glyoxal, sulfur dioxide, carbon monoxide, isoprene, ammonia, and aerosol optical depth, along with the height of aerosol layers associated with traffic, power plants, and wildfires, among other sources. Some of these observations will support emissions updates, while other observations serve as inputs for initial conditions of the model. For example, studies show that the hourly observations from geostationary sensors can produce up-to-date

Table 6. Summary of air quality application areas and observables from GeoXO instruments, with the primary instrument used for retrievals identified by different fonts: ACX in regular weight, GXI in boldface, and GXS in italics.

Application area	Satellite products
Near-real-time emissions monitoring	NO_2, CH_2O, *CO*, SO_2
Air quality forecasting	O_3, NO_2, CH_2O, *CO*, SO_2, $C2H_2O_2$, **AOD**, UV AOD, **$PM_{2.5}$**, aerosol layer height
Air quality monitoring	O_3, NO_2, CH_2O, *CO*, SO_2, $C2H_2O_2$, CO, **AOD**, UV AOD, **$PM_{2.5}$**, **aerosol imagery**, UV aerosol index, aerosol layer height
Fire weather forecasting	**Fire detections**, **fire radiative power**, smoke plume height
Fire emissions monitoring	**Fire detections**, **fire radiative power**
Hazards forecasting	**Fire detections**, **dust detection**, **smoke detection**, SO_2, **volcanic ash**
Greenhouse gas monitoring	*CO_2*, O_3
Stratospheric ozone monitoring	O_3 vertical profile
Climate modeling and Earth system modeling	NO_2, *CO*, O_3, O_3 profile, CH_2O, AOD, *NH_3*, *isoprene*, *N_2O*, stratospheric aerosols, TOA radiation, land cover, UVAOD, aerosol layer height, **fire detection**, **fire radiative power**, smoke injection height, **dust detection**, **volcanic ash**, solar-induced fluorescence

emissions inputs more quickly that the once-a-day observations from polar-orbiting satellites and can lead to improved model forecasts (Hsu et al. 2023).

The GeoXO ACX boundary layer ozone, nitrogen dioxide, and surface $PM_{2.5}$ concentration products will be key for air quality monitoring and related environmental justice applications. Nitrogen dioxide (NO_2), a surrogate for nitrogen oxides (NO_x = NO + NO_2), is released during the combustion of fossil fuels and is a precursor for both ozone and particulate matter, the primary components of photochemical smog, and all three of these pollutants are regulated by the U.S. Environmental Protection Agency. Whether NO_x enhances or decreases ozone production is dependent on a given region having an excess of NO_x or volatile organic compounds (VOCs), due to the inherent nonlinearity of ozone photochemistry (Kroll et al. 2020). The two main sources of NO_x in the United States are the energy sector and the transportation sector according to the 2014 Community Emissions Data System (Hoesly et al. 2018). The LMX also will contribute to air quality monitoring. Kang et al. (2020) described the impacts of lightning NO_x emissions on O_3 air quality, and found that summertime surface O_3 levels in the U.S. Mountain West region can be significantly influenced by lightning NO_x. NO_2, a contributor to the formation of near-surface ozone and aerosols, has harmful direct human health impacts when inhaled. Achakulwisut et al. (2019) showed that 64% of 4 million pediatric asthma cases each year are due to exposure to NO_2. With hourly observations of NO_2 from ACX, this analysis could be expanded to understand the impact of short-term exposure as well as informing the public in a timely manner so that health risks can be minimized.

While plans are underway to use the current ABI-based hourly estimates of surface $PM_{2.5}$ in nowcasting mode to provide alerts and warnings of harmful levels of fine particulate pollution, aerosol composition and layer height information from GeoXO will add value. For instance, uncertainties in estimated $PM_{2.5}$ could be minimized by knowing the height at which an aerosol layer is present in the atmosphere which can change from hour to hour due to meteorological conditions (Fig. 5). If aerosols are present in the elevated layers of the atmosphere, they do not impact air quality at the nose level, i.e., in the air that people actually breathe. The GeoXO ACX instrument adds several new capabilities for NOAA that have never been done with fleet of satellites in LEO. NASA's TEMPO, a pathfinder mission for GeoXO ACX, is setting precedents for capabilities such as boundary layer ozone (the partial column between the surface and 2 km altitude), aerosol layer height, and many related trace gases that are critical for air quality monitoring and forecasting. NOAA is partnering with NASA to use TEMPO

products in an operational setting for day 1 readiness of ACX when GeoXO-Center launches. By combining ACX and GXI data, $PM_{2.5}$ estimated from aerosol optical depth can be parsed into its components from smoke, dust, and anthropogenic sources at an hourly cadence. This capability is important to understand how different regions in the United States are impacted by different source sectors, resulting in knowledge that could transfer into policy recommendations for mitigation strategies at the state and local levels.

Ocean applications. The OCX instrument attributes (Table 3) will lead to (i) more accurate and timely forecasts of coastal phenomena, (ii) improved guidance to state and local agencies to improve mitigation efforts in coastal areas, and (iii) improved predictive models to guide sustainable fishing activities and avoiding bycatch of protected resources. The addition of an ocean color sensor will greatly improve our ability to monitor transient oceanographic features on the time scales in which they occur. OCX's observational capability is optimized to address applications that impact coastal communities. Numerous examples exist ranging from the monitoring of oil spills, HABs, water quality/clarity, and nuisance macroalgae, such as *Sargassum* in tropical waters, to enhanced characterization of indices (i.e., primary productivity) diagnostic of important conditions related to valuable fisheries. In the following sections, we will provide two examples as to how OCX will support and improve fisheries and coastal applications.

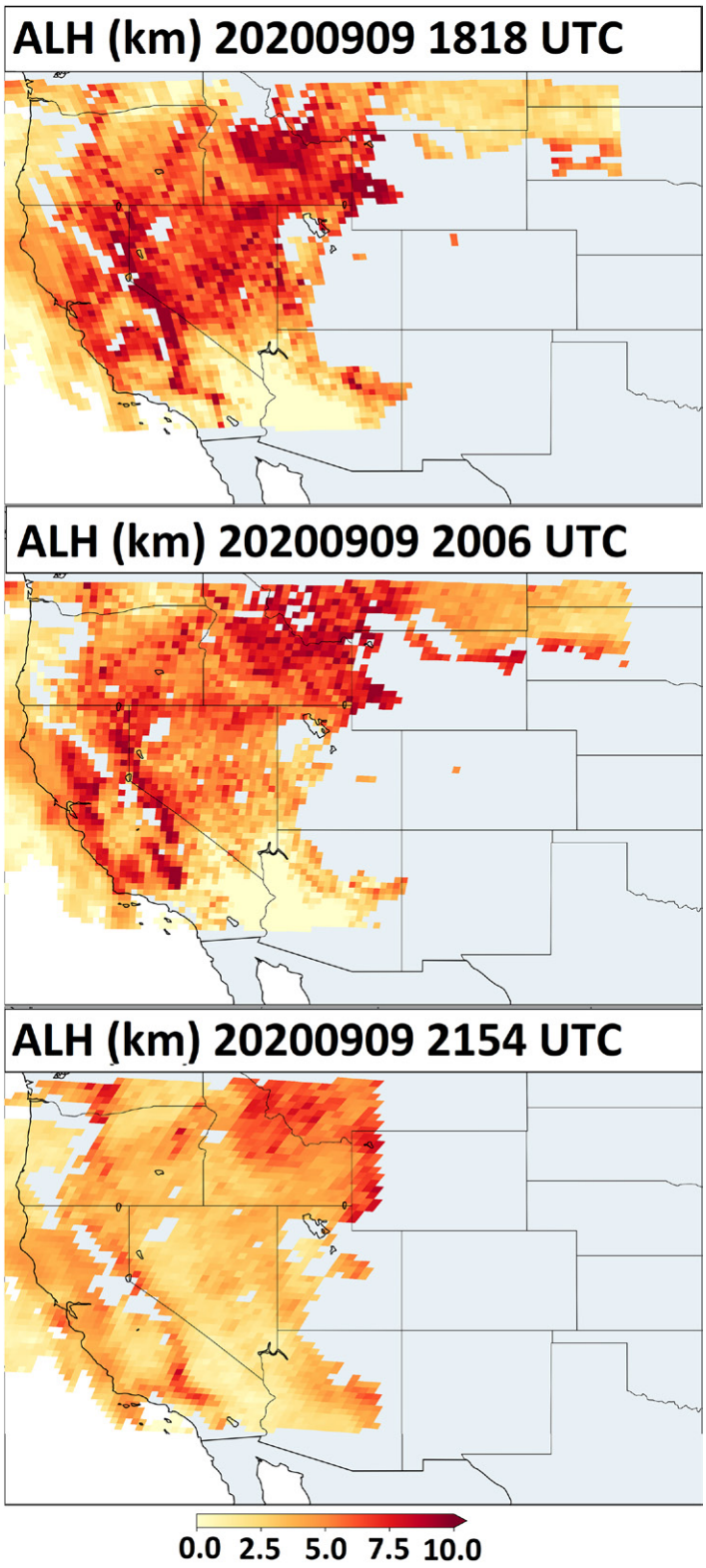

Fig. 5. GeoXO ACX aerosol layer height (ALH) derived using DSCOVR/EPIC as a proxy during a wildfire smoke event on 9 Sep 2020 for three different hours: (top) 1818, (middle) 2006, and (bottom) 0254 UTC.

Harmful algal bloom monitoring and forecasting. NOAA provides HAB forecasts around the United States and ocean color imagery to support monitoring both coastal HABs and

cyanobacterial blooms which affect every U.S. state. The impacts of HABs include illness in both humans and wildlife as a result of their ability to produce neurotoxins. Costs due to a single HAB-related public health event are on the order of millions of U.S. dollars, and acute health effects from HABs and pathogens are estimated to be over $1 billion per year (Ford and Tomlinson 2021). Some HABs can severely impact aquaculture applications by killing juvenile shellfish. Toxic cyanobacteria can cause taste and odor issues, and if not treated, toxins in public drinking water. Dodds et al. (2008) estimated combined costs in U.S. freshwaters of approximately $2.2 billion annually due to losses in recreational water usage, waterfront real estate, recovery of threatened endangered species, and drinking water associated with eutrophication. $813 million alone was attributed to the purchase of bottled water associated with taste and water issues that can be associated with cyanobacteria. In addition, high concentrations of phytoplankton can cause deleterious impacts to coastal ecosystems.

One example of an operational HAB forecast system that relies heavily on ocean color imagery is produced for Lake Erie. The Lake Erie forecast provides the current extent and 4-day outlook of cyanobacterial bloom trajectory and concentration (Fig. 6). Through a combination of ocean color imagery from the European Ocean Colour Land Imager (OLCI) and 3D models, the forecast supports public drinking water managers and the fishing and tourism industries. Due to the frequency of the Sentinel-3 overpasses, coverage over Lake Erie is approximately daily (with a gap every 3 days). Given cloud and glint issues, this is insufficient to get a clear picture of the distribution and magnitude of cyanobacteria. Due to the presence of gas vacuoles, *Microcystis aeruginosa*, the causative organism, can move up and down in the water column in response to nutrients and light (Paerl and Huisman 2008). As a result, the timing of satellite overpass and the peak bloom on a given day is not always synchronized. Having more scenes throughout the day with OCX, forecasts will have more information on the quantity and distribution of *M. aeruginosa* and will provide more accurate information on when toxic algae may be approaching a recreational beach or water intake, influencing important management decisions. Similar examples exist in other coastal and freshwater systems where HABs are a problem.

Improvement to fisheries management. The OCX instrument will have tremendous value in fisheries research and in the proper assessment of fishery resources in relation to physical

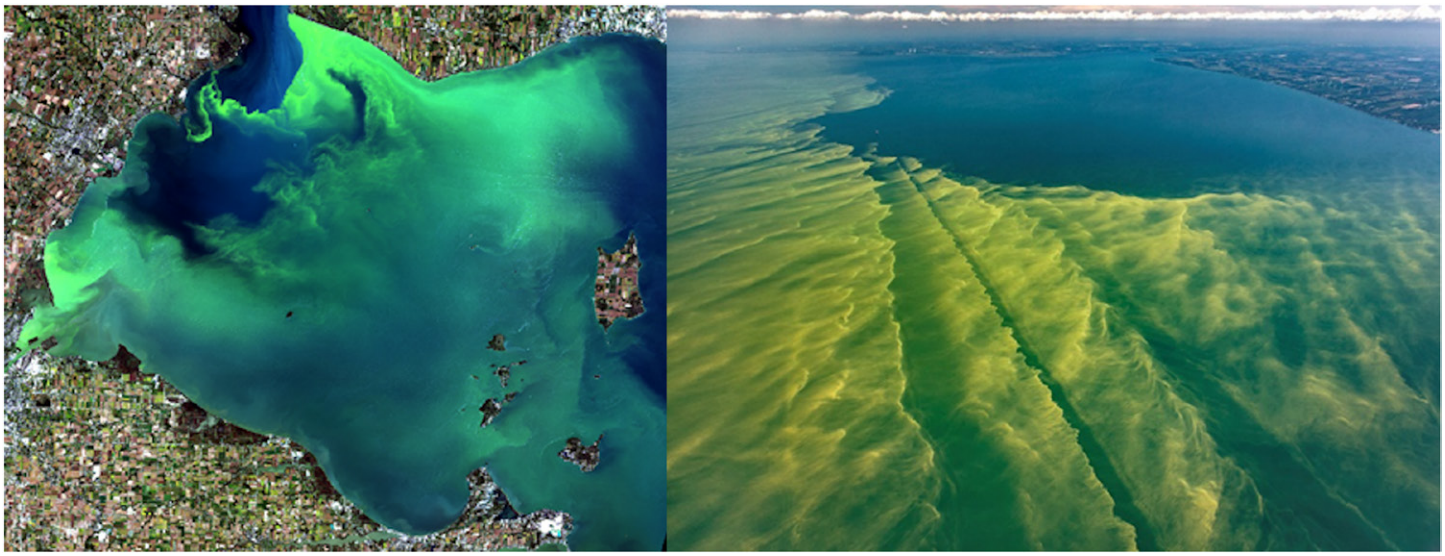

Fig. 6. Cyanobacteria bloom in western Lake Erie, United States. (left) An approximate true color image taken on 26 Sep 2017 by the *Landsat 8* Operational Land Imager (OLI processed by NOAA's National Centers for Coastal Ocean). Bright green water indicates the extent of the bloom in the western basin. (right) The bloom meeting the Detroit River plume from the same time period. Photo credit: Zachary Haslick, Aerial Associates Photography.

and environmental forcing. As noted above, additional information about phytoplankton diversity can be derived from hyperspectral measurements, providing fisheries-critical information on seeding trophic energy potentials in end-to-end ecosystem models (Caracappa et al. 2022), as well as predicting potential disruptions to food web dynamics (do Rosário Gomes et al. 2014). To be robust and informative, marine ecosystem models additionally require parameterized biophysical relationships that rely on realistic water column characteristics at appropriate spatial and temporal scales. Notably, many important processes impacting e.g., where fish congregate, like frontal boundaries and water convergence zones (i.e., submesoscale processes), occur at scales that are pervasively challenging to predict in hydrodynamic forecasting models (Lévy et al. 2018; Dohan and Maximenko 2010). These physical processes can additionally inform direct mechanistic connections between oceanographic phenology to ecosystem development (Schroeder et al. 2014) as well as animal growth and survival rates (Fiechter et al. 2015). The observational capacity of OCX will not only provide an opportunity to validate these regional models at matching scales, but may also enable the direct derivation of high-resolution surface currents from sequential imagery (Sun et al. 2016; Liu et al. 2017) for model assimilation and improvement (IOCCG 2012).

Another useful application for geostationary ocean color is in the Dynamic Ocean Management of living marine resources. Operational systems in NOAA Fisheries assess biophysical ocean conditions to predict favorable habitats of targeted aquatic species, providing modeling capabilities to help reduce bycatch (EcoCast; Hazen et al. 2018) and mitigate interactions with migratory endangered species (WhaleWatch; Hazen et al. 2017). Unfortunately, the ultimate factor limiting near-real-time capabilities is the retrieval of gap-filled ocean color products. To achieve ample signal and mitigate cloud cover, these products either rely on longer temporal composites of ocean color (8 days to 1 month) or are modified to bypass consideration of ocean color altogether to meet operational demands. The temporal cadence of OCX data will support dynamic ocean management, enabling observations that are as fluid in time and space as the managed resources.

Numerical weather prediction. Currently, data from the ABI is assimilated into numerical weather prediction (NWP) models in a few different ways. Observed ABI radiances themselves are assimilated, and clouds are tracked in order to estimate atmospheric motion vectors (AMVs) which are assimilated. These data sources for NWP will continue and likely be improved from GXI. But the major leap forward will come from the assimilation of hyperspectral radiances from GXS. A set of simulations by NASA's Global Modeling and Assimilation Office (GMAO) has shown the GXS will improve forecasts, even out to 3–5 days (McGrath-Spangler et al. 2022). These results are likely an under representation of the true impact due to an older data assimilation system that was used, spectrally thinning of the data, and other assumptions. Additionally, papers by Yin et al. (2021), Ma et al. (2021), Clarisse et al. (2021), Feng et al. (2022), Zhou et al. (2023), Di et al. (2021), Smith et al. (2020), Wang et al. (2021), Okamoto et al. (2020), Li et al. (2018), Jones et al. (2017), Wang et al. (2013), Li et al. (2011), Lin et al. (2017), Santek et al. (2019), Velden et al. (2017), and Adkins et al. (2021) have shown significant improvements expected from GXS or similar sounders with respect to atmospheric and composition forecasts. These studies include both data experiments with actual on-orbit measurements from the Geostationary Interferometric Infrared Sounder (GIIRS) and simulations [traditional Observing System Simulation Experiments (OSSEs), hybrid OSSEs, and quick OSSEs]. In addition to radiance assimilation, work at the European Centre for Medium-Range Weather Forecasts (ECMWF) has shown comparable impact when assimilating retrieved profiles of water vapor (Salonen and McNally 2020), and Kong et al. (2022) have demonstrated positive results when assimilating GLM data.

Climate. GeoXO will contribute in three main ways to the climate mission. It will extend the GOES climate records of clouds (Stubenrauch et al. 2013), surface temperature and radiative fluxes (Meng et al. 2003), precipitation (Adler et al. 2003), aerosol (Prados et al. 2007), and fire (Prins et al. 1998). Second, GeoXO will continue the new climate records established with GOES-R. These include space-based optical lightning and new imager data records such as vegetation indices, aerosol size, and highly spatially and temporally resolved cloud and moisture properties. Last, GeoXO will initiate many new records that will be immediately relevant to climate monitoring and process study communities. These new records include air quality data from ACX and GXS, diurnally resolved coastal ocean color products, and diurnally resolved temperature and moisture profiles.

It is also important to realize that GeoXO will be part of a GEO-RING of similar capabilities from other space agencies and much of its climate impact will be realized as part of this global constellation. For example, GeoXO will allow for the records established by the pioneering GEO-RING International Satellite Cloud Climatology Project (ISCCP; Rossow and Schiffer 1999) started in 1983 to continue. In addition, GeoXO will contribute to new GEO-RING projects such as the next generation of ISCCP (ISCCP-NG), which will exploit the advanced spatial, temporal, and spectral capabilities of all of the geostationary imagers circling the equator to make enhanced cloud, aerosol, and surface products.

Concluding remarks

A new generation of NOAA geostationary satellites only deploys about every two decades, and plans made now will affect the observations collected as late as the mid-2050s. Therefore, decisions on the future constellation must be made carefully and with significant forethought. This is not an easy task considering the changing climate and continued rapid improvements in technology. After significant user engagement efforts, studies with industry, and discussions with both national and international stakeholders, NOAA is moving forward with a constellation that continues imaging and lightning mapping, and adds hyperspectral sounding, ocean color, and atmospheric composition capabilities. The first GeoXO satellite is expected to launch in 2032. Between now and then, research and development will be supported to develop new and innovative applications of these datasets. In addition, user readiness activities will be a priority with a goal of utilizing the data flow on day 1.

GeoXO's new and improved observations from geostationary orbit will join those from low-Earth orbit and together revolutionize numerical weather prediction, hazardous weather monitoring, ocean and air quality observations, and climate monitoring. LEO data are global in nature so includes critical data from over the high latitudes and both the Western and Eastern Hemispheres, while the geostationary data will provide low latency, frequently updating looks at areas in and around North and South America.

Delivery of GeoXO data to users will change significantly compared to the current GOES-R model, in particular by making heavy use of cloud services. GeoXO data products will be available directly from the NOAA National Environmental Satellite, Data, and Information Service (NESDIS) Common Cloud Framework (NCCF). NCCF is a suite of services that allows NESDIS to provide end-to-end ground service capabilities to ingest, process, analyze, distribute, and store all types of NESDIS data for faster, easier dissemination of data to NESDIS partners and users. GeoXO data will be sent directly from the NCCF to the weather and forecasting, oceans, and climate communities via low-latency dissemination service. GeoXO data will also be made available to the public through a consolidated storefront portal where users can search across all NESDIS archived data. Radio frequency broadcast of a subset of the instrument data will be provided through a commercial satellite broadcast. Details on these services will be provided as they become available.

Last, in order to maximize the impact of the observations provided by GeoXO, engagement of the collective weather, oceans, and climate communities is essential. We encourage our user community to explore the applications of these improved and new observations to benefit our society and planet.

Acknowledgments. The authors thank the editor and three anonymous reviewers for significantly improving this manuscript. The authors also thank Jun Wang and Zhendong Lu (University of Iowa) for support with the EPIC aerosol layer height retrieval work; Mat Gunshor (University of Wisconsin–Madison/CIMSS) for Fig. 3, and Hai Zhang (IMSG) for Fig. 5. The views, opinions, and findings contained in this report are those of the authors and should not be construed as an official National Oceanic and Atmospheric Administration or United States Government position, policy, or decision.

Data availability statement. This manuscript describes a *future* satellite system, and although the details of the data distribution and archival are still to be determined, it is expected that all data will be free and open after the satellites are declared operational.

References

Achakulwisut, P., M. Brauer, P. Hystad, and S. C. Anenberg, 2019: Global, national, and urban burdens of paediatric asthma incidence attributable to ambient NO_2 pollution: Estimates from global datasets. *Lancet Planet. Health*, **3**, e166–e178, https://doi.org/10.1016/S2542-5196(19)30046-4.

Adkins, J., and Coauthors, 2021: Geostationary Extended Observations (GeoXO) hyperspectral InfraRed sounder value assessment report. NOAA/NESDIS Tech. Rep., 103 pp., https://doi.org/10.25923/7zvz-fv26.

Adler, R. F., and Coauthors, 2003: The version-2 Global Precipitation Climatology Project (GPCP) monthly precipitation analysis (1979–present). *J. Hydrometeor.*, **4**, 1147–1167, https://doi.org/10.1175/1525-7541(2003)004<1147:TVGPCP>2.0.CO;2.

Anthes, R. A., and Coauthors, 2019: Developing priority observational requirements from space using multi-attribute utility theory. *Bull. Amer. Meteor. Soc.*, **100**, 1753–1774, https://doi.org/10.1175/BAMS-D-18-0180.1.

Aumann, H. H., and R. J. Pagano, 1994: Atmospheric infrared sounder on the Earth Observing System. *Opt. Eng.*, **33**, 776–784, https://doi.org/10.1117/12.159325.

Aurin, D., A. Mannino, and B. Franz, 2013: Spatially resolving ocean color and sediment dispersion in river plumes, coastal systems, and continental shelf waters. *Remote Sens. Environ.*, **137**, 212–225, https://doi.org/10.1016/j.rse.2013.06.018.

Caracappa, J. C., and Coauthors, 2022: A northeast United States Atlantis marine ecosystem model with ocean reanalysis and ocean color forcing. *Ecol. Modell.*, **471**, 110038, https://doi.org/10.1016/j.ecolmodel.2022.110038.

Chen, X., and Coauthors, 2021: First retrieval of absorbing aerosol height over dark target using TROPOMI oxygen B band: Algorithm development and application for surface particulate matter estimates. *Remote Sens. Environ.*, **265**, 112674, https://doi.org/10.1016/j.rse.2021.112674.

Clarisse, L., M. Van Damme, D. Hurtmans, B. Franco, C. Clerbaux, and P.-F. Coheur, 2021: The diel cycle of NH3 observed from the FY-4A Geostationary Interferometric Infrared Sounder (GIIRS). *Geophys. Res. Lett.*, **48**, e2021GL093010, https://doi.org/10.1029/2021GL093010.

Courrèges-Lacoste, G. B., M. Sallusti, G. Bulsa, G. Bagnasco, B. Veihelmann, S. Riedl, D. J. Smith, and R. Maurer, 2017: The Copernicus Sentinel 4 mission: A geostationary imaging UVN spectrometer for air quality monitoring. *Proc. SPIE*, **10423**, 1042307, https://doi.org/10.1117/12.2282158.

Di, D., J. Li, Z. Li, J. Li, T. J. Schmit, and W. P. Menzel, 2021: Can current hyperspectral infrared sounders capture the small scale atmospheric water vapor spatial variations? *Geophys. Res. Lett.*, **48**, e2021GL095825, https://doi.org/10.1029/2021GL095825.

Dierssen, H. M., S. G. Ackleson, K. E. Joyce, E. L. Hestir, A. Castagna, S. Lavender, and M. A. McManus, 2021: Living up to the hype of hyperspectral aquatic remote sensing: Science, resources and outlook. *Front. Environ. Sci.*, **9**, 649528, https://doi.org/10.3389/fenvs.2021.649528.

Dodds, W. K., W. W. Bouska, J. L. Eitzmann, T. J. Pilger, K. L. Pitts, A. J. Riley, J. T. Schloesser, and D. J. Thornbrugh, 2008: Eutrophication of U.S. freshwaters: Analysis of potential economic damage. *Environ. Sci. Technol.*, **43**, 12–19, https://doi.org/10.1021/es801217q.

Dohan, K., and N. Maximenko, 2010: Monitoring ocean currents with satellite sensors. *Oceanography*, **23** (4), 94–103, https://doi.org/10.5670/oceanog.2010.08.

do Rosário Gomes, H., J. I. Goes, S. G. P. Matondkar, E. J. Buskey, S. Basu, S. Parab, and P. Thoppil, 2014: Massive outbreaks of Noctiluca scintillans blooms in the Arabian Sea due to spread of hypoxia. *Nat. Commun.*, **5**, 4862, https://doi.org/10.1038/ncomms5862.

Duncan, B. N., and Coauthors, 2010: Application of OMI observations to a space-based indicator of NO_x and VOC controls on surface ozone formation. *Atmos. Environ.*, **44**, 2213–2223, https://doi.org/10.1016/j.atmosenv.2010.03.010.

Eyre, J. R., W. Bell, J. Cotton, S. J. English, M. Forsythe, S. B. Healy, and E. G. Pavelin, 2022: Assimilation of satellite data in numerical weather prediction. Part II: Recent years. *Quart. J. Roy. Meteor. Soc.*, **148**, 521–556, https://doi.org/10.1002/qj.4228.

Feng, J., X. Qin, C. Wu, P. Zhang, L. Yang, X. Shen, W. Han, and Y. Liu, 2022: Improving typhoon predictions by assimilating the retrieval of atmospheric temperature profiles from the FengYun-4A's Geostationary Interferometric Infrared Sounder (GIIRS). *Atmos. Res.*, **280**, 106391, https://doi.org/10.1016/j.atmosres.2022.106391.

Fiechter, J., and Coauthors, 2015: Environmental conditions impacting juvenile Chinook salmon growth off central California: An ecosystem model analysis. *Geophys. Res. Lett.*, **42**, 2910–2917, https://doi.org/10.1002/2015GL063046.

Ford, M., and M. Tomlinson, 2021: The value of geostationary ocean color. NOAA Tech. Rep., 30 pp., https://repository.library.noaa.gov/view/noaa/33278.

Frost, G. J., and Coauthors, 2020: A value assessment of an atmospheric composition capability on the NOAA Next-Generation Geostationary and Extended Orbits (GEO-XO) missions. NOAA Tech. Rep. OAR CPO-8, 70 pp., https://doi.org/10.25923/1s4s-t405.

GBD 2019 Risk Factors Collaborators, 2020: Global burden of 87 risk factors in 204 countries and territories, 1990–2019: A systematic analysis for the Global Burden of Disease Study 2019. *Lancet*, **396**, 1223–1249, https://doi.org/10.1016/S0140-6736(20)30752-2.

Glumb, R. J., and J. P. Predina, 2002: The Cross-track Infrared Sounder: Sensor design and projected performance. *Proc. 12th Int. ATOVS Study Conf.*, Lorne, VIC, Australia, International TOVS Working Group, 5b2, https://itwg.ssec.wisc.edu/conferences/past-itsc-meetings/itsc-12-program/.

Goodman, S. J., and Coauthors, 2013: The GOES-R Geostationary Lightning Mapper (GLM). *Atmos. Res.*, **125–126**, 34–49, https://doi.org/10.1016/j.atmosres.2013.01.006.

——, T. J. Schmit, J. Daniels, W. Denig, and K. Metcalf, 2019: GOES: Past, present and future. *Comprehensive Remote Sensing*, Vol. 1, Elsevier, 119–149, https://doi.org/10.1016/B978-0-12-409548-9.10315-X.

Groom, S., and Coauthors, 2019: Satellite ocean colour: Current status and future perspective. *Front. Mar. Sci.*, **6**, 485, https://doi.org/10.3389/fmars.2019.00485.

Gurka, J. J., and G. J. Dittberner, 2001: The next generation GOES instruments: Status and potential impact. *Fifth Symp. on Integrated Observing Systems*, Albuquerque, NM, Amer. Meteor. Soc., 7.9, https://ams.confex.com/ams/annual2001/techprogram/paper_17401.htm.

Hazen, E. L., and Coauthors, 2017: WhaleWatch: A dynamic management tool for predicting blue whale density in the California Current. *J. Appl. Ecol.*, **54**, 1415–1428, https://doi.org/10.1111/1365-2664.12820.

——, and Coauthors, 2018: A dynamic ocean management tool to reduce bycatch and support sustainable fisheries. *Sci. Adv.*, **4**, eaar3001, https://doi.org/10.1126/sciadv.aar3001.

Hoesly, R. M., and Coauthors, 2018: Historical (1750–2014) anthropogenic emissions of reactive gases and aerosols from the Community Emissions Data System (CEDS). *Geosci. Model Dev.*, **11**, 369–408, https://doi.org/10.5194/gmd-11-369-2018.

Holmlund, K., and Coauthors, 2021: Meteosat Third Generation (MTG): Continuation and innovation of observations from geostationary orbit. *Bull. Amer. Meteor. Soc.*, **102**, E990–E1015, https://doi.org/10.1175/BAMS-D-19-0304.1.

Hsu, C., and Coauthors, 2024: An observing system simulation experiment analysis of how well geostationary satellite trace-gas observations constrain NOx emissions in the US. *J. Geophys. Res. Atmos.*, **129**, e2023JD039323, https://doi.org/10.1029/2023JD039323.

IOCCG, 2012: Ocean-colour observations from a geostationary orbit. D. Antoine, Ed., IOCCG Rep. 12, 110 pp., https://ioccg.org/wp-content/uploads/2015/10/ioccg-report-12.pdf.

Jin, X., A. Fiore, K. F. Boersma, I. D. Smedt, and L. Valin, 2020: Inferring changes in summertime surface ozone–NO_x–VOC chemistry over US urban areas from two decades of satellite and ground-based observations. *Environ. Sci. Technol.*, **54**, 6518–6529, https://doi.org/10.1021/acs.est.9b07785.

Jolliff, J. K., M. D. Lewis, S. Ladner, and R. L. Crout, 2019: Observing the ocean submesoscale with enhanced-color GOES-ABI visible band data. *Sensors*, **19**, 3900, https://doi.org/10.3390/s19183900.

Jones, T. A., S. Koch, and Z. Li, 2017: Assimilating synthetic hyperspectral sounder temperature and humidity retrievals to improve severe weather forecasts. *Atmos. Res.*, **186**, 9–25, https://doi.org/10.1016/j.atmosres.2016.11.004.

Kang, D., R. Mathur, G. A. Pouliot, R. C. Gilliam, and D. C. Wong, 2020: Significant ground-level ozone attributed to lightning-induced nitrogen oxides during summertime over the Mountain West states. *npj Climate Atmos. Sci.*, **3**, 6, https://doi.org/10.1038/s41612-020-0108-2.

Kim, J., and Coauthors, 2020: New era of air quality monitoring from space: Geostationary Environment Monitoring Spectrometer (GEMS). *Bull. Amer. Meteor. Soc.*, **101**, E1–E22, https://doi.org/10.1175/BAMS-D-18-0013.1.

Kondragunta, S., Z. Wei, B. C. McDonald, D. L. Goldberg, and D. Q. Tong, 2021: COVID-19 induced fingerprints of a new normal urban air quality in the United States. *J. Geophys. Res. Atmos.*, **126**, e2021JD034797, https://doi.org/10.1029/2021JD034797.

——, ——, H. Zhang, H. Liu, I. Laszlo, B. Zhang, C. Cao, and P. Ciren, 2023: Markers of economic activity in satellite aerosol optical depth data. *Environ. Res. Lett.*, **18**, 084013, https://doi.org/10.1088/1748-9326/ace466.

Kong, R., M. Xue, C. Liu, A. O. Fierro, and E. R. Mansell, 2022: Development of new observation operators for assimilating GOES-R geostationary lightning mapper flash extent density data using GSI EnKF: Tests with two convective events over the United States. *Mon. Wea. Rev.*, **150**, 2091–2110, https://doi.org/10.1175/MWR-D-21-0326.1.

Kroll, J. H., C. L. Heald, C. D. Cappa, D. K. Farmer, J. L. Fry, J. G. Murphy, and A. L. Steiner, 2020: The complex chemical effects of COVID-19 shutdowns on air quality. *Nat. Chem.*, **12**, 777–779, https://doi.org/10.1038/s41557-020-0535-z.

Lévy, M., P. J. Franks, and K. S. Smith, 2018: The role of submesoscale currents in structuring marine ecosystems. *Nat. Commun.*, **9**, 4758, https://doi.org/10.1038/s41467-018-07059-3.

Li, F., X. Y. Zhang, S. Kondragunta, X. Lu, I. Csiszar, and C. Schmidt, 2022: Hourly biomass burning emissions product from blended geostationary and polar-orbiting satellites for air quality forecasting applications. *Remote Sens. Environ.*, **281**, 113237, https://doi.org/10.1016/j.rse.2022.113237.

Li, J., J. Li, J. Otkin, T. J. Schmit, and C.-Y. Liu, 2011: Warning information in a pre-convection environment from the geostationary advanced infrared sounding system – A simulation study using IHOP case. *J. Appl. Meteor. Climatol.*, **50**, 776–783, https://doi.org/10.1175/2010JAMC2441.1.

Li, Z., and Coauthors, 2018: Value-added impact of geostationary hyperspectral infrared sounders on local severe storm forecasts—Via a quick regional OSSE. *Adv. Atmos. Sci.*, **35**, 1217–1230, https://doi.org/10.1007/s00376-018-8036-3.

Lin, H., S. S. Weygandt, A. H. Lim, M. Hu, J. M. Brown, and S. G. Benjamin, 2017: Radiance preprocessing for assimilation in the hourly updating rapid refresh mesoscale model: A study using AIRS data. *Wea. Forecasting*, **32**, 1781–1800, https://doi.org/10.1175/WAF-D-17-0028.1.

Liu, J., W. J. Emery, X. Wu, M. Li, C. Li, and L. Zhang, 2017: Computing ocean surface currents from GOCI ocean color satellite imagery. *IEEE Trans. Geosci. Remote Sens.*, **55**, 7113–7125, https://doi.org/10.1109/TGRS.2017.2741924.

Ma, Z., and Coauthors, 2021: Four-dimensional wind fields from geostationary hyperspectral infrared sounder radiance measurements with high temporal resolution. *Geophys. Res. Lett.*, **48**, e2021GL093794, https://doi.org/10.1029/2021GL093794.

Maier, M. W., and Coauthors, 2021: Architecting the future of weather satellites. *Bull. Amer. Meteor. Soc.*, **102**, E589–E610, https://doi.org/10.1175/BAMS-D-19-0258.1.

McGrath-Spangler, E. L., W. McCarty, N. C. Privé, I. Moradi, B. M. Karpowicz, and J. McCorkel, 2022: Using OSSEs to evaluate the impacts of geostationary infrared sounders. *J. Atmos. Oceanic Technol.*, **39**, 1903–1918, https://doi.org/10.1175/JTECH-D-22-0033.1.

——, N. C. Privé, B. M. Karpowicz, I. Moradi, and A. K. Heidinger, 2024: Using OSSEs to evaluate GXS impact in the context of international coordination. *J. Atmos. Oceanic Technol.*, **41**, 261–278, https://doi.org/10.1175/JTECH-D-23-0141.1.

Meng, C. J., R. T. Pinker, J. D. Tarpley, and I. Laszlo, 2003: A satellite approach for estimating regional land surface energy budget for GCIP/GAPP. *J. Geophys. Res.*, **108**, 8861, https://doi.org/10.1029/2002JD003088.

Menzel, W. P., T. J. Schmit, P. Zhang, and J. Li, 2018: Satellite-based atmospheric infrared sounder development and applications. *Bull. Amer. Meteor. Soc.*, **99**, 583–603, https://doi.org/10.1175/BAMS-D-16-0293.1.

Miller, N. B., M. M. Gunshor, A. J. Merrelli, T. S. L'Ecuyer, T. J. Schmit, J. J. Gerth, and N. J. Gordillo, 2022: Imaging considerations from a geostationary orbit using the short wavelength side of the mid-infrared water vapor absorption band. *Earth Space Sci.*, **9**, e2021EA002080, https://doi.org/10.1029/2021EA002080.

Montanyà, J., and Coauthors, 2022: Potential use of space-based lightning detection in electric power systems. *Electr. Power Syst. Res.*, **213**, 108730, https://doi.org/10.1016/j.epsr.2022.108730.

Nanda, S., M. de Graaf, J. P. Veefkind, M. Sneep, M. ter Linden, J. Sun, and P. F. Levelt, 2020: A first comparison of TROPOMI aerosol layer height (ALH) to CALIOP data. *Atmos. Meas. Tech.*, **13**, 3043–3059, https://doi.org/10.5194/amt-13-3043-2020.

Okamoto, K., and Coauthors, 2020: Assessment of the potential impact of a hyperspectral infrared sounder on the Himawari follow-on geostationary satellite. *SOLA*, **16**, 162–168, https://doi.org/10.2151/sola.2020-028.

Paerl, H. W., and J. Huisman, 2008: Blooms like it hot. *Science*, **320**, 57–58, https://doi.org/10.1126/science.1155398.

Prados, A. I., S. Kondragunta, P. Ciren, and K. R. Knapp, 2007: GOES Aerosol/Smoke Product (GASP) over North America: Comparisons to AERONET and MODIS observations. *J. Geophys. Res.*, **112**, D15201, https://doi.org/10.1029/2006JD007968.

Prins, E. M., J. M. Feltz, W. P. Menzel, and D. E. Ward, 1998: An overview of GOES-8 diurnal fire and smoke results for SCAR-B and the 1995 fire season in South America. *J. Geol. Res.*, **103**, 31 821–31 835, https://doi.org/10.1029/98JD01720.

Quesada-Ruiz, S., and Coauthors, 2020: Benefit of ozone observations from Sentinel-5P and future Sentinel-4 missions on tropospheric composition. *Atmos. Meas. Tech.*, **13**, 131–152, https://doi.org/10.5194/amt-13-131-2020.

Rossow, W. B., and R. A. Schiffer, 1999: Advances in understanding clouds from ISCCP. *Bull. Amer. Meteor. Soc.*, **80**, 2261–2288, https://doi.org/10.1175/1520-0477(1999)080<2261:AIUCFI>2.0.CO;2.

Ruddick, K., G. Neukermans, Q. Vanhellemont, and D. Jolivet, 2014: Challenges and opportunities for geostationary ocean colour remote sensing of regional seas: A review of recent results. *Remote Sens. Environ.*, **146**, 63–76, https://doi.org/10.1016/j.rse.2013.07.039.

Rudlosky, S., S. Goodman, K. Calhoun, C. Schultz, A. Back, B. Kuligowski, S. Stevenson, and C. Gravelle, 2020: Geostationary lightning mapper value assessment. NOAA Tech. Rep. NESDIS 153, 46 pp., https://repository.library.noaa.gov/view/noaa/27429.

Salonen, K., and A. McNally, 2020: MTG-IRS Level 2 data assimilation into the ECMWF model. EUMETSAT Tech. Rep. EUM/CO/15/4600001613/TA, 29 pp., www-cdn.eumetsat.int/files/2020-07/pdf_ss_iasi_l2_ecmwf_final_rep.pdf.

Santek, D., S. Nebuda, and D. Stettner, 2019: Demonstration and evaluation of 3D winds generated by tracking features in moisture and ozone fields derived from AIRS sounding retrievals. *Remote Sens.*, **11**, 2597, https://doi.org/10.3390/rs11222597.

Schmit, T. J., W. F. Feltz, W. P. Menzel, J. Jung, A. P. Noel, J. N. Heil, J. P. Nelson III, and G. S. Wade, 2002: Validation and use of GOES sounder moisture information. *Wea. Forecasting*, **17**, 139–154, https://doi.org/10.1175/1520-0434(2002)017<0139:VAUOGS>2.0.CO;2.

——, M. M. Gunshor, W. P. Menzel, J. J. Gurka, J. Li, and A. S. Bachmeier, 2005: Introducing the next-generation Advanced Baseline Imager (ABI) on GOES-R. *Bull. Amer. Meteor. Soc.*, **86**, 1079–1096, https://doi.org/10.1175/BAMS-86-8-1079.

——, J. Li, S. A. Ackerman, and J. J. Gurka, 2009: High-spectral- and high-temporal-resolution infrared measurements from geostationary orbit. *J. Atmos. Oceanic Technol.*, **26**, 2273–2292, https://doi.org/10.1175/2009JTECHA1248.1.

——, P. Griffith, M. M. Gunshor, J. M. Daniels, S. J. Goodman, and W. J. Lebair, 2017: A closer look at the ABI on the GOES-R series. *Bull. Amer. Meteor. Soc.*, **98**, 681–698, https://doi.org/10.1175/BAMS-D-15-00230.1.

——, S. S. Lindstrom, J. J. Gerth, and M. M. Gunshor, 2018: Applications of the 16 spectral bands on the Advanced Baseline Imager (ABI). *J. Oper. Meteor.*, **6**, 33–46, https://doi.org/10.15191/nwajom.2018.0604.

Schroeder, I. D., and Coauthors, 2014: Application of a data-assimilative regional ocean modeling system for assessing California Current System ocean conditions, krill, and juvenile rockfish interannual variability. *Geophys. Res. Lett.*, **41**, 5942–5950, https://doi.org/10.1002/2014GL061045.

Silvern, R. F., and Coauthors, 2019: Using satellite observations of tropospheric NO_2 columns to infer long-term trends in US NO_x emissions: The importance of accounting for the free tropospheric NO_2 background. *Atmos. Chem. Phys.*, **19**, 8863–8878, https://doi.org/10.5194/acp-19-8863-2019.

Smith, W. L., Sr., Q. Zhang, M. Shao, and E. Weisz, 2020: Improved severe weather forecasts using LEO and GEO satellite soundings. *J. Atmos. Oceanic Technol.*, **37**, 1203–1218, https://doi.org/10.1175/JTECH-D-19-0158.1.

Stevenson, S. N., K. L. Corbosiero, M. DeMaria, and J. L. Vigh, 2018: A 10-year survey of tropical cyclone inner-core lightning bursts and their relationship to intensity change. *Wea. Forecasting*, **33**, 23–36, https://doi.org/10.1175/WAF-D-17-0096.1.

Streets, D. G., and Coauthors, 2013: Emissions estimation from satellite retrievals: A review of current capability. *Atmos. Environ.*, **77**, 1011–1042, https://doi.org/10.1016/j.atmosenv.2013.05.051.

Stubenrauch, C. J., and Coauthors, 2013: Assessment of global cloud datasets from satellites: Project and database initiated by the GEWEX radiation panel. *Bull. Amer. Meteor. Soc.*, **94**, 1031–1049, https://doi.org/10.1175/BAMS-D-12-00117.1.

Sun, H., Q. Song, R. Shao, and T. Schlicke, 2016: Estimation of sea surface currents based on ocean colour remote-sensing image analysis. *Int. J. Remote Sens.*, **37**, 5105–5121, https://doi.org/10.1080/01431161.2016.1226526.

Suomi, V. E., and R. J. Parent, 1968: A color view of planet Earth. *Bull. Amer. Meteor. Soc.*, **49**, 74–75, https://doi.org/10.1175/1520-0477-49.2.74.

Tong, D. Q., and Coauthors, 2015: Long-term NO_x trends over large cities in the United States during the great recession: Comparison of satellite retrievals, ground observations, and emission inventories. *Atmos. Environ.*, **107**, 70–84, https://doi.org/10.1016/j.atmosenv.2015.01.035.

Vandermeulen, R. A., A. Mannino, A. Neeley, J. Werdell, and R. Arnone, 2017: Determining the optimal spectral sampling frequency and uncertainty thresholds for hyperspectral remote sensing of ocean color. *Opt. Express*, **25**, A785–A797, https://doi.org/10.1364/OE.25.00A785.

Velden, C., W. E. Lewis, W. Bresky, D. Stettner, J. Daniels, and S. Wanzong, 2017: Assimilation of high-resolution satellite-derived atmospheric motion vectors: Impact on HWRF forecasts of tropical cyclone track and intensity. *Mon. Wea. Rev.*, **145**, 1107–1125, https://doi.org/10.1175/MWR-D-16-0229.1.

Wang, H., X.-Y. Huang, and Y. Chen, 2013: An observing system simulation experiment for the impact of MTG candidate infrared sounding mission on regional forecasts: System development and preliminary results. *ISRN Meteor.*, **2013**, 971501, https://doi.org/10.1155/2013/971501.

Wang, P., Z. Li, J. Li, and T. J. Schmit, 2021: Added value of GEO-Hyperspectral infrared radiances for local severe storm forecasts using hybrid OSSE method. *Adv. Atmos. Sci.*, **38**, 1315–1333, https://doi.org/10.1007/s00376-021-0443-1.

Weaver, J. F., D. Lindsey, D. Bikos, C. C. Schmidt, and E. Prins, 2004: Fire detection using GOES rapid scan imagery. *Wea. Forecasting*, **19**, 496–510, https://doi.org/10.1175/1520-0434(2004)019<0496:FDUGRS>2.0.CO;2.

Weisz, E., and W. P. Menzel, 2022: Tracking atmospheric moisture changes in convective storm environments using GEO ABI and LEO CrIS data fusion. *Remote Sens.*, **14**, 5327, https://doi.org/10.3390/rs14215327.

Westerling, A. L., 2016: Increasing western US forest wildfire activity: Sensitivity to changes in the timing of spring. *Philos. Trans. Roy. Soc.*, **B371**, 20150178, https://doi.org/10.1098/rstb.2015.0178.

Williams, A. P., J. T. Abatzoglou, A. Gershunov, J. Guzman-Morales, D. A. Bishop, J. K. Balch, and D. P. Lettenmaier, 2019: Observed impacts of anthropogenic climate change on wildfire in California. *Earth's Future*, **7**, 892–910, https://doi.org/10.1029/2019EF001210.

Yin, R., W. Han, Z. Gao, and J. Li, 2021: Impact of high temporal resolution FY-4A Geostationary Interferometric Infrared Sounder (GIIRS) radiance measurements on typhoon forecasts: Maria (2018) case with GRAPES global 4D-Var assimilation system. *Geophys. Res. Lett.*, **48**, e2021GL093672, https://doi.org/10.1029/2021GL093672.

Zhou, K., L. Ran, L. Zhou, T. Zhao, L. Chen, and H. Liu, 2023: The study of Fengyun4A temperature profile data assimilation in a southwest vortex heavy rainfall case. *Atmos. Res.*, **283**, 106566, https://doi.org/10.1016/j.atmosres.2022.106566.

Zhu, L., and Coauthors, 2016: Observing atmospheric formaldehyde (HCHO) from space: Validation and intercomparison of six retrievals from four satellites (OMI, GOME2A, GOME2B, OMPS) with SEAC4RS aircraft observations over the southeast US. *Atmos. Chem. Phys.*, **16**, 13 477–13 490, https://doi.org/10.5194/acp-16-13477-2016.

Ziemke, J. R., and Coauthors, 2019: Trends in global tropospheric ozone inferred from a composite record of TOMS/OMI/MLS/OMPS satellite measurements and the MERRA-2 GMI simulation. *Atmos. Chem. Phys.*, **19**, 3257–3269, https://doi.org/10.5194/acp-19-3257-2019.

Zoogman, P., and Coauthors, 2017: Tropospheric emissions: Monitoring of pollution (TEMPO). *J. Quant. Spectrosc. Radiat. Transfer*, **186**, 17–39, https://doi.org/10.1016/j.jqsrt.2016.05.008.